Journal Name

Dynamic Article Links ►

"This document is the Accepted Manuscript version of a Published Work that appeared in final form in Nanoscale, copyright © Royal Society of Chemistry after peer review and technical editing by the publisher. To access the final edited and published work see Nanoscale, 2014, 6, 316."

www.rsc.org/xxxxxx ARTICLE TYPE

Correlating Elastic Properties and Molecular Organization of an Ionic Organic Nanostructure

Jeremy R. Eskelsen,[a] Yun Qi,[b] Samantha K. Schmitt,[c] K. W. Hipps*[a], and Ursula Mazur*[a]

Received (in XXX, XXX) Xth XXXXXXXXX 20XX, Accepted Xth XXXXXXXXX 20XX

DOI: 10.1039/b000000x

Mechanical and structural properties of ionically self-assembled nanostructures of meso-tetra(4-sulfonatophenyl)porphyrin (TSPP) and meso-tetra(4-pyridyl)porphyrin (TPyP) are presented. This is the first time that elastic modulus of an ionic porphyrin solid has been reported. X-ray photoelectron spectroscopy (XPS), UV-visible spectra, and elemental analysis all support a stoichiometric 1:1 TSPP to TPyP composition. Atomic force microscopy (AFM), revealed that the porphyrin nanostructure is composed of stacked ribbons about 20 nm tall, 70 nm wide, and several microns in length. High resolution transmission electron microscopy (HRTEM) images showed clear lattice fringes 1.5±0.2 nm in width aligned along the length of the nanorod. Selected area electron diffraction (SAED) and powder x-ray diffraction patterns of TSPP:TPyP support an orthorhombic system and space group Pmm2 with lattice parameters a = 26.79 Å, b = 20.00 Å, and c = 8.42 Å. Crystallographic data is consistent with an arrangement of alternating face-to-face TSPP and TPyP molecules forming ordered columns along the length of the nanorods. The structural integrity of the solid is attributed to combined noncovalent interactions that include ionic, hydrogen bonding, and π-π interactions. The values of Young's modulus obtained for the crystalline TSPP:TPyP nanorods averaged 6.5 ± 1.3 GPa. This modulus is comparable to those reported for covalently bonded flexible polymeric systems. The robust bonding character of the TSPP:TPyP nanostructures combined with their mechanical properties makes them excellent candidates for flexible optoelectronic devices.

Introduction

One of the most important advantages of organic molecular semiconductors over their inorganic equivalents is that their electronic, mechanical, and optical properties can be chemically tuned by molecular design. This advantage can be further enhanced by arranging the individual photo- and electro-active molecules into organized assemblies that possess charge carrier properties superior to those of their corresponding bulk forms.[1,2] The molecular interactions that mediate the optoelectronic properties of organic nanomaterials are also known to have pronounced effects on their mechanical properties such as elastic modulus, hardness, and bending strength.[3,4,5] For high performance practical applications of organic semiconducting nanostructures (light-emitting diodes,[6] field-effect transistors,[7] photoswitches,[1] sensors,[8,9] solar cells,[10,11] and memory devices[12]) fast and efficient carrier mobility needs to be coupled with low internal stress and superior tensile characteristics.[13] For example, both increased elastic modulus and conductivity were observed for polypyrrole nanotubes with improved longitudinal alignment of the polymer chains via π-π interactions.[5] Metal-like stiffness and transparent optical properties were reported for nanospheres formed from aromatic dipeptides.[14] The rigid geometry of the nanospheres was constrained by efficient aromatic interactions and a network of hydrogen bonded carboxylate groups. Accordingly, good fundamental understanding of structure – property relationships is crucial in designing and building high performance, stable, and durable molecular devices and remains one of the key scientific challenges for advancing organic optoelectronic technology.

In this report, we present a detailed structural study and elastic properties of a porphyrin based nanostructure with focuses on the structure – property relationship of this system. Synthetic porphyrins are an important class of organic semiconductors that structurally and functionally resemble natural light harvesting chromophores and they are promising building blocks for organic electronics,[15] photovoltaics,[16,17] sensors,[8,18,19] and catalysts.[20] Porphyrin nanostructures may be prepared by a variety of methods including ionic self-assembly,[21,22] phase-transfer ionic self-assembly,[23] surfactant-assisted self-assembly,[24] and vapour condensation recrystallization.[25] Of particular interest to us are the porphyrin nanostructures created by ionic self-assembly, a rather simple solution-based synthetic method that utilizes a combination of structurally different ionic species, or a single zwitterionic species.[26-31] Nanostructures composed from oppositely charged porphyrin ions (also called cooperative binary ionic, CBI, solids) are particularly appealing because they present a novel class of robust nanomaterials that have been shown to potentially serve as efficient light-harvesting

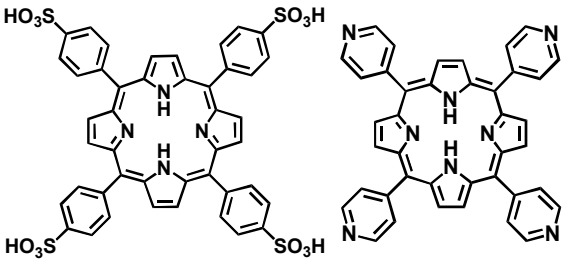

Fig. 1 Free- base forms of meso-tetra(4-sulfonatophenyl)porphyrin, TSPP, left , and of meso-tetra(4-pyridyl)porphyrin, TPyP, right.

components of dye-sensitized solar cells and organic photovoltaics. [26,32] Favorable optoelectronic properties of some of the reported CBI solids may be attributed, in part, to their reported crystalline character[26,32] It is well known that organic molecular crystals exhibit higher charge mobility than amorphous and polycrystalline films and are therefore better candidates for the fabrication of high-performance electronic and optical devices.[2,4,33] For example, copper phthalocyanine (CuPc) crystalline (β-phase) nanowires have higher charge mobility then films fabricated from the same compound.[4] Nanometer size crystals, like the CBI systems, are especially attractive because they may possess fewer defects and grain boundaries that can act as energetic barriers for charge transport. In addition, the reduced dimensions of nanocrystals may impart better flexibility, a highly desirable mechanical property for high-performance flexible molecular optoelectronic devices.[34,35] To date there has been little reported on the mechanical properties of porphyrin materials and, to our knowledge, no mechanical measurements available for ionic porphyrin nanostructures. Similarly, there is a scarcity of detailed molecular and submolecular structural data on the CBI systems.[36,37] The main reason for the lack of structural data is because the size of the CBI crystals that can be isolated are at best suitable for powder and not single crystal X–ray diffraction. To date only one crystal structure of a single CBI solid prepared from zinc(II) tetra(4-sulfonatophenyl)-porphyrin (ZnTPPS) and tin(IV) tetra(N-methyl-4-pyridiniumyl)porphyrin (SnTNMePyP) has been reported.[32]

The subject of this report is a binary system formed from metal free porphyrin tectons namely, meso-tetra(4-pyridyl)porphyrin, TPyP, and meso-tetra(4-sulfonatophenyl)porphyrin, TSPP, Fig. 1. It is important to note that solution pH plays a significant role in determining the numbers of protons (and therefore the charge) of these tectons. We will use the TSPP and TPyP notation for brevity, but will also identify the actual protonation state when needed. The TSPP:TPyP CBI material was prepared earlier but its stoichiometric and structural details are unknown. [26,38] A combination of spectroscopic and microscopic analysis here furnishes a detailed molecular level model of how the TSPP and TPyP ionic tectons combine in the CBI nanostructure. X-ray photoelectron spectroscopy (XPS), electronic spectroscopy, atomic force microscopy (AFM), high resolution transmission electron microscopy (HRTEM), selected area electron diffraction (SAED), powder X-ray diffraction (XRD), and DFT calculations helped us to model the structure and organization of molecules within the nanostructured aggregates. XPS was particularly useful in identifying the protonation (via shifts in the N 1s peak) states of the TSPP and TPyP tectons, their stoichiometry in the ionically coupled solid, and the elemental composition of the porphyrin nanocomposite. Morphology and dimensions of the rod-like structures were acquired from their AFM images. HRTEM, SAED, and X-ray powder patterns were used to establish the crystallinity of the TSPP:TPyP nanorods and molecular orientation within nanostructured aggregates. The collective application of spectroscopy and microscopy furnished a detailed molecular level picture of how the TSPP and TPyP ionic tectons combine in the CBI nanostructure.

Young's modulus (E) measurements of the TSPP:TPyP nanostructures were made using an AFM by applying a force to the nanorods while measuring the corresponding indentation. Both highly ordered pyrolytic graphite (HOPG) and mica substrates were used to test if the elastic modulus values of the nanostructures were affected by the underlying substrate. E showed no substrate dependence at the depth of indent studied and no degradation of the porphyrin nanorods was observed after repeated deformation. The values of the Young's modulus obtained for the crystalline ionic TSPP:TPyP nanorods were comparable to those of covalently bonded polymeric systems but are an order of magnitude smaller than that of inorganic nanowires[39] making them excellent candidates for flexible optoelectronic devices.

Experimental section

TSPP:TPyP nanostructure synthesis. The procedure for the preparation and isolation of the solid nanomaterial is described in the Supplemental Information. Therein also are the solution electronic spectra of the TSPP:TPyP aggregates.

Atomic Force Microscopy. AFM measurements were taken, using a Digital Instruments Multimode AFM in tapping mode. Silicon cantilevers with a driving frequency around 300 MHz and a force constant of 42 N/m were used in the measurement of the AFM images. Substrates for imaging were highly oriented pyrolytic graphite (HOPG) and mica purchased from SPI Supplies Inc. AFM samples were prepared by depositing 1-2 drops by Pasteur pipette of the TSPP/TPyP aggregate solution onto freshly peeled mica or HOPG for 1 minute followed by a 30 second spin at 3900 rpm. This process was repeated 10 times.

Helium Ion Microscopy. Samples for HIM were prepared in the same fashion as for the AFM and were checked by AFM prior to imaging by HIM. The microscope used was an ORION® PLUS manufactured by Carl Zeiss located at Pacific Northwest National Lab in Richland, WA. The ORION® He ion microscope is capable of imaging with two different detectors, an Everhart-Thornley and a Rutherford backscattering detector. The Everhart-Thornley detector measures secondary electrons ejected from the sample by the incident He ions, while the Rutherford backscattering detector measures He ions scattered by the sample nuclei. Both modes were used to analyze the nanorods.

TEM, HRTEM, and SAED. For transmission electron microscopy and high resolution imaging, nanorods were

This journal is © The Royal Society of Chemistry [year]

deposited onto Ni Formvar TEM grids for 1 min followed by wicking using the edge of a paper filter. All images were acquired using a Philips CM200 TEM at an acceleration voltage of 200 keV and outfitted with a controlled eucentric sample holder capable of a tilt from - 45º to + 45º along the A axis and -30º to +30º along the B axis. The SAED of the nanorods was also determined using the CM200 with line resolution of 0.19 nm with the same holder.

XRD. X-ray powder diffraction data was gathered using a Rigaku MiniFlex 600 by Lori Fields Hatherley at Rigaku Americas Corporation. The sample was placed in a 0.2 mm deep, zero background holder. Copper Kα X-rays at 40 kV and 15 mA emission, with a scintillation detector and graphite monochromator were used for the analysis. A θ/2θ scan was ran from 2° to 60° with a step size of 0.02° and a 15 sec/pt dwell time. The total time for analysis was 12.1 hours.

Le Bail refinement and modelling. The CMPR program was used to obtain a starting space group and lattice dimensions.[40] The lattice constants were then refined via a Le Bail fit[41] in the program GSAS interfaced by EXPGUI.[42,43] Peak profiles were modelled with a pseudo-Voigt peak shape[44] with the Finger, Cox, Jephcoat asymmetry function[45] to deal with the low-angle data. An 8-term shifted Chebyschev polynomial was used to model the amorphous background. S/L and H/L values were set at 0.005. The parameters refined were the lattice parameters and the peak shape parameters *u*, *v*, *w*, and *x*. The u, v, and w parameters were refined separately to prevent refining out of bounds. The constraints are u and w > 0 and v < 0. The total number of parameters refined was 12, not including the background. We modeled the crystal structure with the refined lattice constants and intermolecular distances for the isolated ions from DFT energy minimized structures. CrystalMaker®: a crystal and molecular structures program for Mac and Windows was used. [46] This model is based on our XPS findings of a 1:1 TSPP:TPyP ratio. Our model correctly reproduces all the data, but it is not a unique solution.

Calculations and modelling. Structural calculations and geometry optimizations of the ionized species were performed using the commercial program Gaussian 03. All reported results are based on DFT calculations using the B3LYP functional and the 6-311G(d,p) basis. (See Supplemental Information for results)

Mechanical measurements. Young's modulus measurements were made using a Bruker Multimode 8 AFM with Nanoscope V controller and a J "vertical" scanner and a lateral force Digital Instruments AFM head. Bruker's Nanoscope 8.15 software was used for the acquisition of data. Two different antimony doped silicon cantilevers with length, resonance frequency, and spring constant values of 116.3 μm, 131.8, kHz, 2.91 N/m and 116.7 μm, 137.9 kHz, 3.65 N/m, respectively, were used for acquiring force-distance curves. Experimental details of the modulus data acquisition and analysis in given in the Supplemental Information.

TSPP:TPyP nanorod solutions were prepared at 15:15 μM porphyrin concentration at pH 2 as described in the Supplemental Information. The AFM samples and substrates were prepared by taping a piece of mica or HOPG to a round AFM puck using double stick tape. A fresh surface of mica or HOPG was exposed by pealing the top layer using adhesive tape. Using a Pasteur pipette, 1-2 drops of the nanorod solution (stirred) was applied to the freshly peeled surface and allowed to remain on the surface for 1 minute followed by spinning at 3800 rpm for 30 seconds. The deposition and spinning was repeated for 5-10 times depending on the substrate and the desired surface coverage. The nanorod surface coverage was inspected under an optical microscope prior to scanning.

Results and discussion

Structural studies

The TSPP:TPyP solid nanostructures were prepared reproducibly in a 1:1 stoichiometric ratio in a pH 2 aqueous HCl solution as based on optical absorption studies and described in the Supplemental Information. At this hydrogen ion solution concentration, the TSPP exists in a diacid form where the inner nitrogen system is protonated and all four sulfonate groups are ionized, to give the porphyrin a net -2 charge, $[H_4TSPP]^{2-}$.[47] The TPyP remains a free base at pH 2.[48] The pyridyl nitrogens in TPyP are commonly believed to be protonated near pH 2.3 based on the measured pK_a value of 5.25 for pyridine in aqueous solutions. [48] To our knowledge, no one has ever measured the pKa of TPyP. Thus, it is possible that there may be a significant concentration of the +2 form of TPyP present at pH 2.

Elemental analysis results summarized in Table 1 readily support the 1:1 composition ratio of TSPP to TPyP found by UV-vis analysis. The expected and experimental proportions of nitrogen to sulfur are exactly 3:1. The measured C:N ratio is slightly greater then the calculated value but could be due to trace carbon contamination. We did observe variable amounts of residual chlorine in our unheated samples but this element was easily removed by heating the solid composite to above 100°C as shown in our XPS results that follow.

In order to verify the stoichiometry of the TSPP:TPyP obtained from above experiments, we performed XPS studies on the nanostructures at room temperature and after heating to 150ºC. Firstly, the nominal amounts of chlorine XPS signal detected in the CBI samples at room temperature were reduced to a negligible level upon heating the sample (see Table 1 and Supplemental Information) indicating that the anion is not an essential constituent of the nanostructures. There was also little evidence of chloride anions found in the EDX spectra of a related CIB nanostructure composed of $[H_4TPPS]^{2-}$ and a tin substituted tetrapyridyl porphyrin, $H_4[SnTPyP]^{4+}$, synthons.[21] The measured N:S and C:N atomic ratios presented in Table 1 agree very well with the calculated atomic ratios consistent with 1:1 tecton stoichiometry. The excellent agreement between the experimental and calculated S:C ratio gives us a great deal of confidence in making this stoichiometric assignment. The slight excess of carbon in the measured C:N ratios in both heated and unheated samples (Table 1) is not surprising, as some background carbon is always present on the indium used to support the compound for XPS analysis. XPS spectra of other pertinent atomic species (Cl and O) present in the tectons are reported in

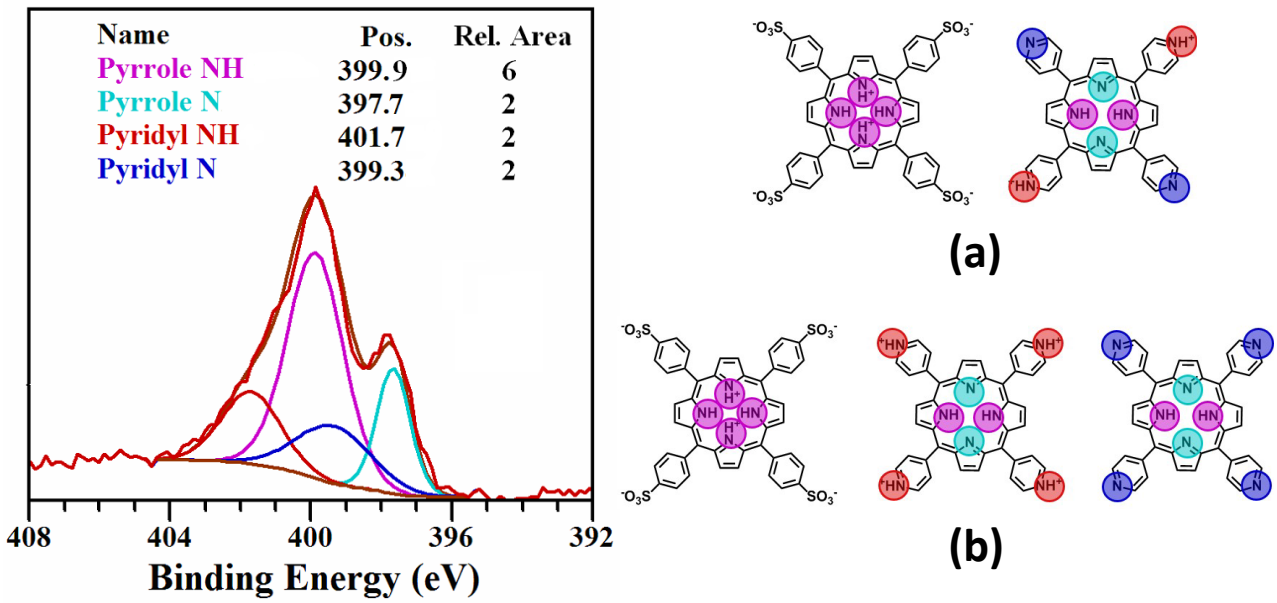

Fig. 2 N1s region XPS for TSPP:TPyP nanorod powder. The colored line fits are associated with the binding energies arising from different types of unprotonated and protonated nitrogens in the porphyrin tecton shown on the right. The relative areas under each curve in the XPS spectra are also given. The possible stoichiometric porphyrin combination are (a) $1[H_4TSPP]^{2-}$: $1H_2[H_2TPyP]^{2+}$ and (b) $2[H_4TSPP]^{2-}$:$1H_4[H_2TPyP]^{4+}$:1 H_2TPyP.

the Supplemental Information. Based on the O 1s XPS, we believe there are 4 waters present per TSPP:TPyP unit in the nanorod annealed to 150ºC.

In addition to assaying elemental content, XPS was also used to evaluate and verify the state of protonation of the inner rings of the tectons in the nanostructures, as shown in Fig. 2. For the TSPP diacid only a single N1s peak is expected at 400 eV, signaling that all four nitrogen atoms of the porphyrin are protonated.[31] The neutral unprotonated H_2[TPyP] should have three types of nitrogen atoms, two unprotonated and two protonated pyrrole N's and four nitrogen atoms in the pyridine rings bound to the porphyrin meso carbons. The reported nitrogen spectrum for this porphyrin vapor deposited on Au(111) showed three overlapping bands.[49,50] This signal was deconvoluted into bands with area ratios of 2:4:2, one located at 399.4 eV, corresponding to the two protonated pyrrole nitrogens, the second one at 398.3 eV corresponding to the four pyridyl nitrogens, and the third one at 397.4 eV corresponding to the two unprotonated pyrrole ring nitrogens.[49,50]

The highest BE signal observed in Fig. 2 is an obvious shoulder at 401.7 eV. This N1s peak position is typical for pyridinium cation nitrogen.[51] We attribute the strong band near 400 eV to the protonated pyrrole nitrogens of the TSPP diacid and the TPyP free base. Also contributing to that signal is the N1s binding energy of the unprotonated pyridyl nitrogens of the TPyP. The 397.7 eV peak is assigned to the unprotonated pyrrole nitrogens in TPyP since the TSPP diacid has all four ring N atoms associated with H atoms. Taking into account the atomic ratio data in Table 1 and guided by previous deconvolution results for the N1s band for neutral TPyP, we have fitted the spectrum in Fig. 2 to four bands associated with four different nitrogens. These bands are linked with the signals from six protonated and two unprotonated pyrrole nitrogens and two protonated and two unprotonated pyridyl nitrogens with relative areas of 6:2:2:2.

Table I. Atomic ratios for 1:1 TSPP:TPyP nanorod stoichiometry obtained from XPS data compared with expected values and elemental analysis results. (*Chlorine signal is barely discernable above the noise level and the values used are probably over estimates.)

Atomic ratios	Calculated	XPS based at 25C	XPS based after heating to 150 C	Elemental analysis
N:S	3:1	3:1	3:1	3:1
C:N	7:1	7.6:1	7.8:1	7.4:1
S:Cl	--	12.2:1*	36.6:1*	variable

Our spectroscopic and elemental analysis data clearly supports 1:1 stoichiometry of TSPP to TPyP in the nanostructure. Since no other ionic species were detected besides a trace of chlorine, and because the relative amounts of the other elements were not significantly altered with heating, we must conclude that the formation of the charge neutral solid can only result from the combination of one $[H_4TSPP]^{2-}$ and one $H_2[H_2TPyP]^{2+}$ ion, or from two$[H_4TSPP]^{2-}$ with one each $H_4[H_2TPyP]^{4+}$ and H_2TPyP. Both tecton combinations preserve the charge neutrality and stoichiometry in the solid state. In a pH 2 solution it is less clear which ionic species combinations predominate.

Interestingly, when $[H_4TPPS]^{2-}$ and $H_4[SnTPyP]^{4+}$ were combined at pH 2 in HCl solution the ratio of the tectons was charge consistent with 2.0–2.5 TSPP to 1 SnTPyP as determined by EDX and optical spectroscopy.[21] Clearly, incorporation of a

This journal is © The Royal Society of Chemistry [year]

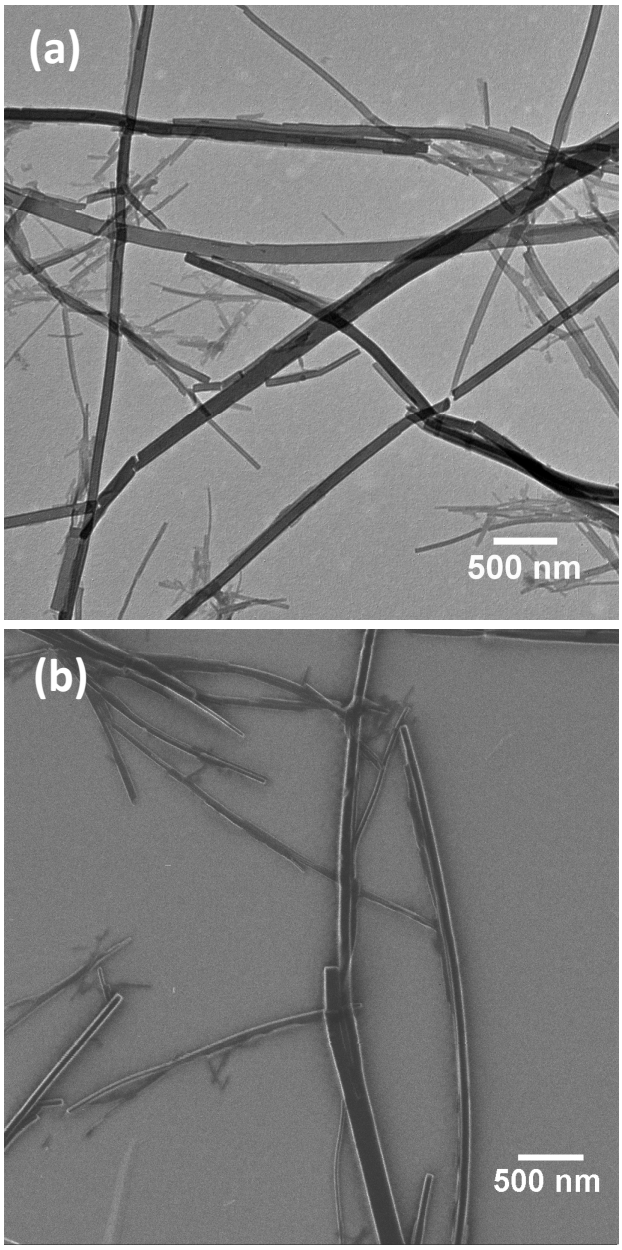

Fig. 3 Low resolution 5 μm x 5 μm images of TSPP:TPyP nanorods on deposited on HOPG acquired by TEM (a) and HIM (b).

metal into the ring of one of the tectons appears to affect charge stabilization on the porphyrins, which in turn affects the stoichiometry of the ionic coupling.

Morphology images from TEM, HIM, and AFM

Previous morphology studies of the TSPP:TPyP aggregates prepared in pH 2 solution reported inconsistent results. One study concluded that TSPP in combination with TPyP forms rods that have a rectangular cross-section and vary considerably in length.[26] Another article claimed that the two tectons formed nanosheets and nanotubes and that the nanotubes resulted from wrapping of the nanosheets.[38]

In Fig. 3 the TEM and HIM images of the TSPP:TPyP system deposited on HOPG reveal rectangular rod-like structures (not collapsed tubes). HIM is a new imaging methodology and we were pleased to discover that the porphyrin nanostructures behaved quite robustly in the ion beam and did not disintegrate even after long exposure times. The edges of the rectangular rods are prominent in the HIM image and corroborate the vertical edges deduced from the TEM results. Our TEM imaging data collected from multiple TSPP:TPyP preparations are consistent with Shelnutt's TEM measurements of the same CBI system.[26] Snitka and coworkers, however, reported that the TSPP:TPyP ionic aggregate formed porphyrin nanosheets with high aspect ratios and multiwall nanotubes, based on their AFM, SEM, and TEM studies.[38] We never observed any of these structures in our TSPP:TPyP samples.

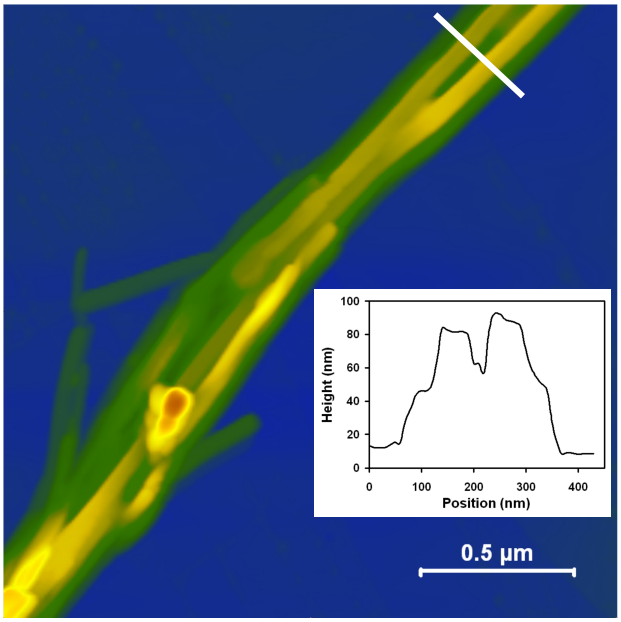

Fig. 4 Ambient tapping mode AFM image of 1:1 TSPP:TPyP deposited onto HOPG reveals large rod-like structures composed of stacked ribbons on the order of a micron in length. Inset shows the line plot across the rod.

While the TEM and HIM images yield good information concerning widths and the lengths of the TSPP/TPyPP nanostructures they provide no height values. Our AFM images provide the first direct evidence that these rods are really composed of overlaid thin strips about 70 nm wide and 20 nm high (Fig. 4). Images acquired from different areas of the same sample, and from different samples, yielded the same nanorod dimensions. The rods are indeed rectangular in shape and have relatively smooth surfaces (see inset in Fig. 4). Rods tend to coalesce into tall stacks tens of nanometers high in the direction of their long axis. Their large size rendered the nanorod stacks unsuitable for imaging by scanning tunnelling microscopy, STM, the technique of choice for probing nano and subnanoscale dimensions. HRTEM, SAED, and powder diffraction patterns, however, allowed us to infer a molecular arrangement within the TSPP:TPyP nanostructures that is consistent with all the available data.

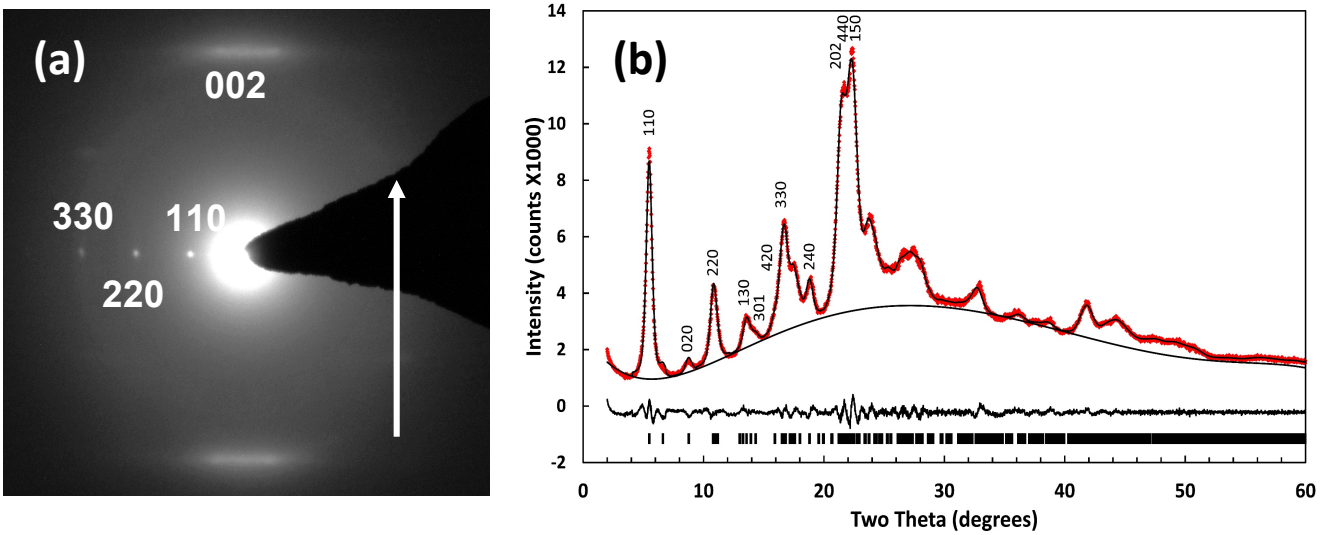

Fig. 5 SAED pattern of a TSPP:TPyP nanorod (a) with Miller indices labels. The arrow identifies z-direction parallel to the substrate surface. In (b) the top trace is the experimental x-ray powder diffraction pattern of TPyP:TSPP nanorods (black curve) with an overlaid Le Bail fit (red doted line) below is the difference trace. At the bottom are the peak locations for a single crystalline phase. Primary peak locations in the powder pattern are labelled.

Nanorod internal structure based on HRTEM, SAED, and powder X-ray diffraction.

HRTEM of the porphyrin nanostructures showed clear fringes indicating that the rods are crystalline as shown in the Supplemental information. The spacing between the lines, 1.5 ± 0.2 nm, is consistent with the distance between two porphyrins positioned side by side with rings in perpendicular orientation relative to the substrate. It is important to note that the morphological and crystallographic properties of the TSPP:TPyP solid were not altered by heating (see Supplemental Information).

Table 2. Comparison of lattice reflection spacings for TPyP:TSPP nanorods from XRPD based on and SAED.

Miller Indices	XRPD Reflection Distances (Å)	SAED Reflection Distances (Å)
110	16.11 ± 0.24	15.3 ± 1.5
220	8.06 ± 0.12	7.7 ± 0.8
330	5.37 ± 0.08	5.2 ± 0.5
440	4.03 ± 0.06	3.8 ± 0.4
002	4.30 ± 0.06	4.5 ± 0.5
004	2.15 ± 0.03	2.2 ± 0.2
130	6.53 ± 0.10	6.9 ± 0.7
020	10.10 ± 0.15	10.8 ± 1.1
040	5.05 ± 0.08	5.5 ± 0.6

The SAED images of the nanorods show a clear crystalline pattern with lattice spacings: d = 1.5 ± 0.2 nm across the width of the rod and d = 0.44 ± 0.08 nm along the length of the rod (Fig. 5a). These spacings are consistent with columns of face-to-face stacked porphyrins aligned parallel to the long axis of the rod (c direction) with the macrocycles lying perpendicular to the substrate surface. The diffuse spots in the SAED scattering can be associated with a small degree of structural disorder in the crystalline nanorods. This disorder may be caused by amorphization of nanomaterial upon exposure to the electron beam, or, more likely by random displacement of the coherent columns of porphyrins relative to each other (in the z-direction) within the nanostructure. Borras et. al. also observed an unperturbed zeroth order diffraction line and diffuse higher order lines in the SAED pattern of vapor deposited crystalline copper phthalocyanine nanowires.[52] They attributed it to random offset in the adjacent phthalocyanine columns in the z-direction (long column axis). Pershan in his review of X-ray scattering from mesomorphic systems noted that X-ray scattering cross sections from disc-shaped molecules with either short or long range ordering usually exhibits a diffuse spot.[53] Thus far, we have been unsuccessful in preparing crystals large enough to obtain a single-crystal X-ray diffraction pattern. We have, however, obtained reproducible powder patterns of several TSPP:TPyP samples, one of which is depicted in Fig. 5b. Table 2 compares the lattice spacings for TPyP:TSPP nanorods obtained from XRPD and SAED. The accuracy of the TEM in general is about 10% to 15%.[54] The accuracy of the powder XRD is not as high as usually expected due to the broadness of the peaks due to the nanocrystalline size and the number of overlapping peaks due to the large lattice spacings. We estimate an error of about 1.5% from multiple attempts at refining the structure. The diffraction pattern is consistent with an orthorhombic crystal system. We have focus on the orthorombic system because related porphyrin systems such as zinc-tetrakis(4-melhoxycarbonylphenyl) porphyrin-pyridine complex[55] and a meso-tetra (N-methy-4-pyridyl)porphyrin tetratosylate and zinc-tetrakis(4-sufonatolphenyl) porphyrin composite[56] were reported

This journal is © The Royal Society of Chemistry [year]

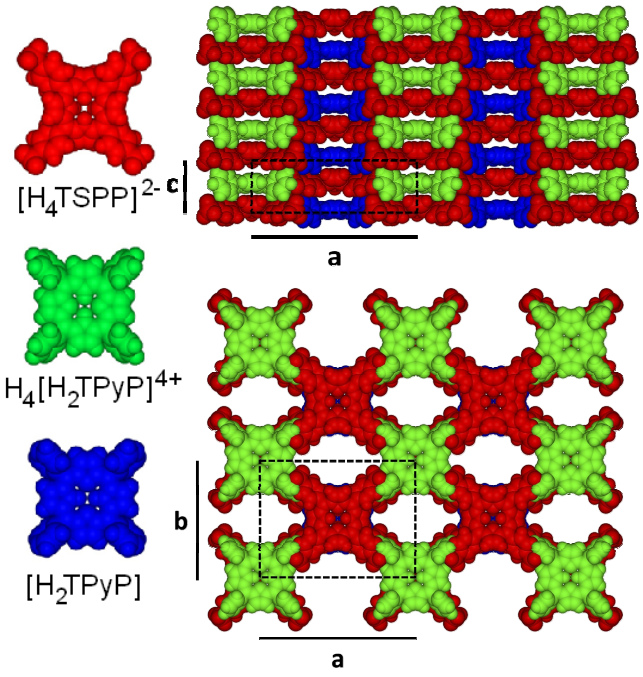

Fig. 6 Model crystal structure based on the ionic tecton ratio $[H_4TSPP]^{2-}$: 1 $H_4[H_2TPyP]^{4+}$:1 $[H_2TPyP]$ and the Pmm2 crystal system. The tectons (on the left) are color coded. Side (down the [200] zone axis) and top (down [002] zone axis) views of crystal structure are presented with the unit cell identified with dashed black lines. The lattice constants are a = 26.71 Å, b = 20.16 Å, and c = 8.61 Å.

to crystallize into an orthorhombic structure. Using a trial space group of Imm2, we obtained lattice parameters a = 26.79 Å, b = 20.00 Å, and c = 8.42 Å using CMPR[40]. The lattice parameters were refined using a Le Bail fit[41] with a reduced X^2 = 2.423 and R_p = 0.0200, see Fig. 5b. The refined lattice constants are a = 26.71 Å, b = 20.16 Å, and c = 8.61 Å.

Using DFT calculated structures of the individual TSPP and TPyP molecules we built an initial model using the refined Imm2 space group. However, the symmetry elements of that group generated a molecular arrangement that was inconsistent with our XPS stoichiometric results. Because a 2 $[H_4TSPP]^{2-}$:1 $H_4[H_2TPyP]^{4+}$: 1 $[H_2TPyP]$ combination is also plausible based on our spectroscopic data we selected a lower symmetry space group, Pmm2, a subgroup of Imm2 to better represent the crystal structure of the nanorods. A structural model of the TSPP:TPyP system based on the Pmm2 group is depicted in Fig. 6. The molecules are arranged with one $[H_4TSPP]^{2-}$ centered at (0, 0, 0), one $[H_4TSPP]^{2-}$ centered at (½, ½, ½), one $H_4[H_2TPyP]^{4+}$ centered at (0, 0, ½), and one $[H_2TPyP]$ centered at (½, ½, 0). Water molecules are present in the nanorod matrix but, for simplicity, they were not included in our crystal structure model. It must also be noted that in the absence of a single crystal diffraction study, a structure consistent with the SAED and powder diffraction is not necessarily the correct structure.

Comparison of SAED data with the powder diffraction supports the arrangement of alternating face-to-face TSPP and TPyP molecules forming columns along the length of the nanorods. Ionic bonding, hydrogen bonding, and π-π interaction each contribute to aligning the ionic tectons (the macrocycles and their ring substituents) in cofacially packed columns, giving the CBI solid a well-defined rod-like structure. Moreover, the HRTEM image of a TSPP/TPyP in Fig. 6a is also compatible with this columnar formation. The well defined striped structure along the nanorod axis is formed by porphyrin columns of an approximate width of 1.5 nm. This value is consistent with a close packed arrangement of the porphyrin tectons (CPK models) depicted in Fig. 6. The dimensions of the individual $[H_4TSPP]^{2-}$, $[H_2TPyP]$, and $H_4[H_2TPyP]^{4+}$ ions are 1.56 nm, 1.20 nm, and 1.23 nm, respectively, based on their calculated equilibrium geometries (See Supporting Information). The $[H_4TSPP]^{2-}$ diacid has 2-fold symmetry because of the distortion (or saddling) in the porphyrin ring caused by inner proton repulsion,[26,29] while the $H_4[H_2TPyP]^{4+}$ and $[H_2TPyP]$ free base species are not significantly distorted. One would expect that in the saddled conformation, the $[H_4TSPP]^{2-}$ macrocycle approaches the $H_4[H_2TPyP]^{4+}$ tecton closer than if both were planar. In fact the separation between the two synthons is small, only 0.43 nm (for reference the porphyrin spacing in Bacteriochlorophyll is 0.35 nm[57]). This is a much shorter distance than the value of 0.689 nm reported for the intermolecular separation of neutral free base tetrapyridyl porphyrins cofacially packed in a monoclinic single crystal.[25] In a 1:1 composite of meso-tetra(N-methyl-4-pyridyl)porphyrin tetratosylate (TMPyP) and ZnTSPP the spacing between the oppositely charged tectons in a face to face arrangement was 0.489 nm based on powder diffraction data.[32] Because of the shorter distance and more ideal bonding angle, the out of plane acidic protons of the $H_2[H_4TSPP]^{2-}$ ring interact strongly with the pyrrolic nitrogens of the $H_4[H_2TPyP]^{4+}$ tecton. The closer macrocycle proximity also facilitates stronger π-π interactions. The sulfonate groups as well as the pyridyl groups on the porphyrin rings can easily adjust themselves to give the maximum ionic and H-bonding.

Elastic modulus measurement

Accurate assessment of the mechanical properties of organic nanostructures such as TSPP:TPyP is complicated by their small physical dimensions and the atomic force microscope is the ideal tool for quantifying the deformation behavior of small volume materials. We employed a Bruker Multimode 8 AFM capable of collecting PeakForce quantitative nanomechanical mapping (PF-QNM) images of surfaces. The elastic property fitting models such as the Derjaguin, Muller, Toporov (DMT)[58] and the Sneddon[59] models are compatible with data acquired with the Bruker Multimode AFM. The DMT model works well for indentation experiments where the tip radius is much greater than the indentation depth.[60] For tip radii much smaller than the indentation depth, the Sneddon model is more appropriate.[61] Typical AFM tip radii used in our experiments were approximately 20 nm. Sample indent depth was limited to 2 nm. Since the tip radius was much larger than the indent depth, the DMT equation was chosen for determining the Young's modulus. See Supplemental Information for detailed experimental procedure of` data acquisition and analysis.

We used two different antimony doped silicon cantilevers with length, resonance frequency, and spring constant values of 116.3 μm, 131.8, kHz, 2.91 N/m and 116.7 μm, 137.9 kHz, 3.65

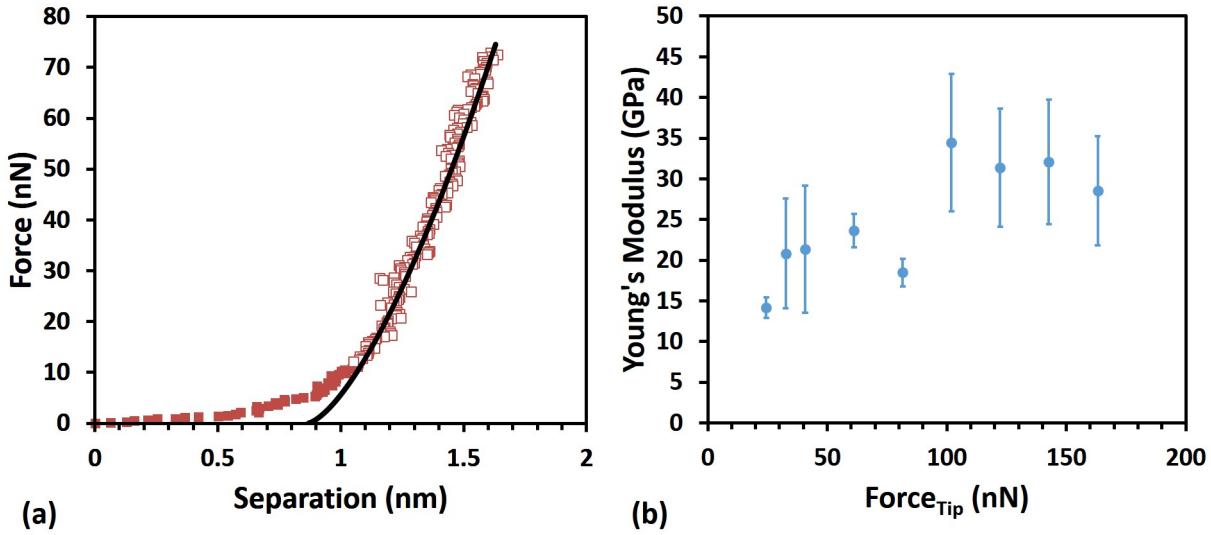

Fig. 7 Young's modulus determination and results for highly ordered pyrolytic graphite (HOPG). (a) Retract curve (red squares) with zero separation set at the point of maximum adhesion: 1 Hz ramp, 750 mV trigger threshold, 200 nm ramp size, 2048 pts per line, 32 degree x-rotate. The red boxes show the top 80 percent fit region. The black line is the DMT (s_m) fitted curve. (b) Young's modulus values on HOPG as a function of maximum tip force (F_{Tip}). Five different ramps at each force value were employed.

N/m, respectively, for acquiring force - displacement curves. The deflection sensitivity of each cantilever was determined by taking single ramps on both sapphire and mica substrates. These substrates are hard materials with Young's modulus values of 441 GPa [62] and 137 GPa,[63] respectively. The spring constants of the AFM cantilevers were determined using the Sader method.[64] In agreement with the literature, the best force – displacement curve measurements were obtained with dulled tips.[65,66]

In order to test the accuracy of our experimental method and calculations employed, we first evaluated the Young's modulus of HOPG using different cantilevers and collecting several measurements with each. Fig. 7 depicts a representative force - displacement curve for HOPG; Young's modulus values of 23 ± 6 GPa and 25 ± 9 GPa were obtained using two different cantilevers. These values fit well into the range of 15-30 GPa reported in the literature for HOPG.[67 68,70]

TPyP:TSPP nanorod samples were deposited on both HOPG and freshly peeled mica. With the AFM in PF-QNM mode, the tip approach to the sample was monitored using the camera on the AFM. The sample was then scanned at a 2 µm scan size with minimal force using Bruker's ScanAsyst. The image was offset until the center of the scan was directly over top of the nanorod and the creep and drift were allowed to settle. Once the creep and drift stabilized, the AFM was switched into ramp mode. Ramp settings were identical to those used for the HOPG indent studies. These settings consisted of five single ramps per deflection error voltage at voltages ranging from 300 to 2000 mV. The TSPP:TPyP sample was imaged again and the tip centered in a different location on either the same or a different nanorod. The same data analysis procedures were used for the nanorod samples as were used on the clean HOPG standard to determine the reduced Young's modulus.

The average values of the Young's modulus obtained for TSPP:TPyP nanorods of variable thickness deposited on HOPG and mica are 6.6 ± 1.3 GPa and 6.4 ± 1.2 GPa respectively (see Fig. 8 and Table 3). Note that in Fig. 8b, the red data points represent the average modulus obtained from only two rod samples. The other *E* data reported in Fig. 8 is based on measurement collected from four or more nanorods. We observed that the modulus for the TSPP:TPyP samples sometimes increased erratically at ramp set points higher than 1000 mV. This may have been a result of a tip shape change. Based on this observation, only the values obtained from ramps measured at 300, 400, 500, 750, and 1000 mV were used in determining the average Young's modulus of each nanorod. The maximum tip force applied to each nanorod ranged from 19-68 nN using the cantilever with a spring constant of 2.91 N/m and 24-82 nN for the cantilever with a spring constant of 3.65 N/m.

It is gratifying that the average values of the elastic modulus of the TSPP:TPyP nanorods deposited on HOPG and on mica are almost identical. In addition, the summary of results in Table 3 shows that the modulus does not seem to correlate with the thickness of the rods. Both of these results indicate that we are truly measuring the mechanical property of the TSPP:TPyP samples and not that the substrates used (HOPG and mica), both of which are much harder materials.

The TSPP:TPyP crystalline nanorods exhibited elastic deformation with a Young's modulus of 6.5 GPa. This value is comparable to that of polyfluoroethylene (7.5 GPa) and is a factor of 2 higher than the modulus for polyethylene (3 GPa). *E* is an intrinsic material property and is fundamentally related to internal bonding properties of the solid. The stronger the intermolecular bonds, the larger the Young's modulus. Table 4 compares the values of Young's modulus for TSPP:TPyP and other organic and inorganic materials. Although the noncovalent interaction in the ionic porphyrin solid are weaker than the covalent bonds in organic polymers their collective contribution gives the self assembled ionic TSPP:TPyP solid excellent structural integrity and *E* values comparable to those of covalently bonded materials.

This journal is © The Royal Society of Chemistry [year]

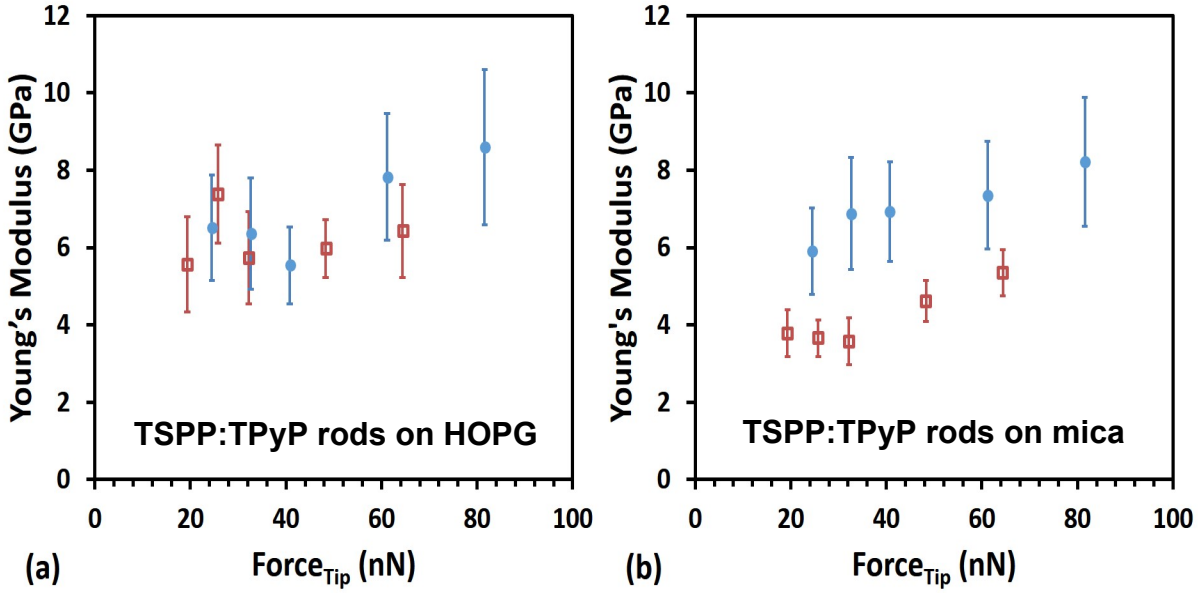

Fig. 8 Average Young's modulus of TSPP:TPyP nanorods obtained using two different cantilevers: 2.91 N/m spring constant (red data) and 3.65 N/m spring constant (blue data). (a) *E* of rods deposited on HOPG. The blue and red data points are the average modulus values acquired from 4 different rods and 5 different ramps at the force value employed. (b) *E* of rods deposited on mica. The blue data are the modulus values obtained from 7 different rods and 5 different ramps at the force value employed. The red graph is a plot of modulus values obtained from 2 different rods and 5 different ramps at the force value employed.

In fact, poor alignment of polymer chains decreases the order in the nanostructures resulting in low values of modulus of elasticity, as in the case of polypyrrole (PPy) nanotubes.[5] alkoxy copper phthalocyanines pCuPc(OOR)$_8$ exhibited unusually high nearly metallic Young's modulus.[63] The strength of these films was determined by the extent of π-π bonds

Table 3. DMT fit of average Young's modulus values obtained for TSPP:TPyP nanorods with different dimensions deposited on HOPG and mica. A total of 13 samples were studied. Appended also are indentation depth and tip radius ranges.

HOPG Substrate				Mica Substrate			
Nanorod Height (nm)	**Average *E* (GPa)**	**Indentation Depth (nm)**	**Tip Radius (nm)**	**Nanorod Height (nm)**	**Average *E* (GPa)**	**Indentation Depth (nm)**	**Tip Radius (nm)**
89[b†]	3.4 ± 0.6	1.0-1.9	21-35	38[b†]	6.0 ± 1.7	0.9-1.7	18-33
89[b†]	4.8 ± 1.7	1.0-1.6	20-32	38[b†]	11.8 ± 2.9	0.5-1.0	9-19
*100[a]	4.0 ± 1.0	0.8-1.2	27-39	62[a]	5.5 ± 1.0	0.7-1.1	25-37
*100[a]	6.8 ± 1.4	0.6-1.1	20-38	62[a]	2.9 ± 0.8	0.8-1.5	29-41
115[a]	9.1 ± 2.2	0.4-0.9	14-33	68[b]	5.3 ± 1.0	0.9-1.5	18-31
135[a]	4.9 ± 2.2	0.6-1.9	22-44	107[b]	3.3 ± 0.5	1.0-1.9	19-34
190[b]	8.2 ± 2.5	0.6-1.1	11-23	220[b†]	6.4 ± 1.6	0.8-1.4	14-28
190[b]	5.7 ± 1.9	0.7-1.4	13-28	220[b†]	7.9 ± 2.4	0.7-1.4	13-29
				220[b†]	8.6 ± 2.4	0.6-1.2	11-24
Average	**6.6 ± 1.3**			**Average**	**6.4 ± 1.2**		

*Approximate nanorod height.
[a]Obtained using a 2.91 N/m cantilever with a range of maximum applied force from 19-68 nN.
[b]Obtained using 3.65 N/m cantilever with a range of maximum applied force from 24-82 nN.
[†]Measurements made on the same nanorod.

Improved ordering of the PPy chains along the nanotube axis resulted in more efficient π-π interactions and fewer defects. The more ordered PPy nanostructures displayed higher elastic modulus and improved charge mobilty.[5] Multilayered Langmuir-Blodgett films made from peripherally substituted interaction in their cofacial arrangement and interdigitation of the long paraffinic chains. Single crystalline nanowires of β phase copper phthalocyanine (CuPc), held together by π-π bonds, were reported to have an elastic modulus of 1.5 GPa.[5] These nanowires were easily bent and relaxed without loosing their

crystalline integrity or decrease in charge mobility.[5] The elasticity and flexibility of CuPc nanowires was attributed to π-π bonding mediated organization of the phthalocyanine cores. The crystalline TSPP:TPyP nanorods have a higher elastic modulus than the CuPc nanowires, almost certainly because, in addition to the aromatic interactions, they also maintain electrostatic and hydrogen bonding. Like the CuPc nanowires, however, the TSPP:TPyP nanorods stiffness values are one order of magnitude smaller than that of inorganic nanowires, indicating that organic nanowire crystals are softer and hence more appropriate for flexible devices. Interestingly, we observed that the TSPP:TPyP are photoconducting i.e., they are insulating in the dark but become conducting under illumination. The results of our photo conductivity studies of the TSPP:TPyP system will be published elsewhere.

Table 4. Comparison of Young's modulus valued for TSPP:TPyP and other materials.

Material	Young's modulus (GPa)
Polypyrrole films[71]	1.2
β-phase CuPc nanowires (AFM)[4]	1.9
Polyformaldehyde[63]	2.9
Polyethylene[72]	3
Polypyrrole nanotubes[5]	1.2 – 3.2
Benzene single crystal (250 K)	5.1
CuPc Film (nanoindenter)[73]	5.2
TSPP:TPyP nanorods/mica (AFM)	6.4 ± 1.2
TSPP:TPyP nanorods/HOPG (AFM)	6.6 ± 1.2
Benzophenone single crystal[74]	6.7
Polyfluoroethylene[75]	7.5
Ammonium sulfate single crystal[74]	23.8
HOPG (AFM)	25 ± 9
ZnTe nanowire[39]	63 ± 6
pCuPc$(OOc)_8$/W (nanoindenter) [63]	83 ± 5.7
Calcium sulfate single crystal[74]	88.3
pCuPc$(OBu)_8$/mica (AFM) [63]	110 ± 15

Conclusions

We have prepared a crystalline porphyrin nanostructure composed of TSPP and TPyP tectons in a one to one stoichiometric ratio. Our AFM images provide the first direct evidence that the nanostructures are rods composed of overlaid thin strips about 70 nm wide and 20 nm high, and on the order of a micron in length. The HRTEM SAED images of the nanorods show a clear crystalline pattern with lattice spacings: d = 1.5 ± 0.2 nm across the width of the rod and d = 0.41 ± 0.08 nm along the length of the rod. The TSPP:TPyP are thermally stable and do not lose their crystallinity when heated to temperatures up to 150C. Comparison of SAED data with the powder x-ray diffraction supports an arrangement of alternating face-to-face TSPP and TPyP molecules forming columns along the length of the nanorods. Ionic bonding, hydrogen bonding, and π-π interactions each contribute to aligning the ionic tectons (the macrocycles and their ring substituents) in cofacially packed columns, giving the CBI solid a well-defined rod-like structure. By correlating the diffraction pattern with the orientation of the nanorods, we arrive at the conclusion that the porphyrins within the columns are stacked perpendicular to the substrate surface and the stacking axis is the long axis of the rod. We are attempting to grow single crystals of the TSPP:TPyP solid to further refine its crystal structure.

The close proximity of the $[H_4TSPP]^{2-}$ and $H_4[H_2TPyP]^{4+}$ or $[H_2TPyP]$ tectons in the nanorod structure is thought to result from the distorted structure of the $[H_4TSPP]^{2-}$ diacid. In its saddled conformation the $[H_4TSPP]^{2-}$ can form strong hydrogen bonds and π-π interactions with the $H_4[H_2TPyP]^{4+}$ and $[H_2TPyP]$ tectons. The low rotational barriers for charged groups on the porphyrin rings allow the sulfonate and the pyridyl substituents on the porphyrin rings to easily adjust their orientation in the TSPP:TPyP composite to maximize the ionic and H-bonding interactions.

We employed AFM based nanoindentation to obtain information on the elastic properties of the TSPP:TPyP nanostructure. By acquiring statically significant sampling of the elastic compliance measurements we have obtained reproducible values of the Young's modulus. The values of *E* obtained for the crystalline TSPP:TPyP nanorods averaged 6.6 ± 1.3 GPa and 6.4 ± 1.2 GPa when deposited on HOPG and mica, respectively, indicating that we are truly measuring the mechanical property of the TSPP:TPyP samples and not that of the substrates. These modulus values are comparable to those reported for covalently bonded flexible polymeric systems and crystalline molecular solids like CuPc and benzophenone. The robust bonding character of the TSPP:TPyP nanostructures combined with their fine elastic properties makes them excellent candidates for flexible optoelectronic devices.

Acknowledgments

This material is based upon work supported by the National Science Foundation under Grants CHE-11152951, CHE-1048600, and DEG-0806677-004. SKS also thanks NSF-REU program Grant DMR-1062898 for funding. We thank the Pacific Northwest National Laboratory for access to their Helium Ion Microscope. We are grateful to the Francheschi Microscopy and Imaging Center at Washington State University for the use of their transmission electron microscopes.

Notes and references

[a] *Department of Chemistry and Materials Science and Engineering Program, Washington State University, PO Box 644630, Pullman, WA, 99164-4630 United States. E-mail: umazur@wsu.edu; Fax: +509-335-886; Tel: +509-335-5822. E-mail: hipps@wsu.edu; Fax: +509-335-886; Tel: +509-335-3033*

[b] *Charles Evans & Associates, Sunnyvale, CA, 9408, United States*

[c] *Department of Material Science and Engineering, University of Wisconsin, Madison, WI, 5370, United States*

This journal is © The Royal Society of Chemistry [year]

† Electronic Supplementary Information (ESI) available: Additional UV-visible data examining the relative stoichiometry involved in forming the TSPP:TPyP binary aggregates at pH 2 as well as additional XPS, diffraction, and nanomechanical data and analysis are given in the ESI. See DOI: 10.1039/b000000x/

References

1 H. Yu, Z. Bao, and J.H. Oh: High-Performance Phototransistors Based on Single-Crystalline n-Channel Organic Nanowires and Photogenerated Charge-Carrier Behaviors. *Adv. Funct. Mater.* **23**, 629–639, (2013).

2 R. Li, W. Hu, Y. Liu, and D. Zhu: Micro- and Nanocrystals of Organic Semiconductors. *Accounts of Chemical Research* **43**, 529-540, (2010).

3 M. Kanan, T. Wakamalsu, R.G.G. Fall, and I. Ihara: Improved Density and Mechanical Properties of a Porous Metal-Free Phthalocyanine Thin Film Isotropically Pressed with Pressure Exceeding the Yield Strength. *Applied Physics Express* **4**, 111603-111603-3, (2011)..

4 Q. Tang, Y. Tong, Y. Zheng, Y. He, Y. Zhang, H. Dong, W. Hu, T. Hassenkam, and T. Bjornholm: Organic Nanowire Crystals Combine Excellent Device Performance and Mechanical Flexibility. *Small* **7**, 189-193, (2011).

5 S. Cuenot, S. Demoustier-Champagne, and B. Nyste: Elastic modulus of polypyrrole nanotubes. *Phys. Rev. Lett.* **85**, 1690-1693, (2000).

6 O. Fenwick, J.K. Sprafke, J. Binas, D.V. Kondratuk, F. Di Stasio, H.L. Anderson, and F. Cacialli: Linear and Cyclic Porphyrin Hexamers as Near-Infrared Emitters in Organic Light-Emitting Diodes. *Nano Lett.* **11**, 2451-2456, (2011).

7 J.S. Jung, J.W. Lee, K. Kim, M.Y. Cho, S.G. Jo, and J. Joo: Rectangular Nanotubes of Copper Phthalocyanine: Application to a Single Nanotube Transistor. *Chem. Mater.* **22**, 2219–2225, (2010).

8 A.B. Braunschweig, A.L. Schmucker, W.D. Wei, and C.A. Mirkin: Nanostructures Enabled by On-Wire Lithography (OWL). Chem. Phys. Lett. ***486****, 89-98, (2010).*

9 C. Di Natalea, D. Monti, and R. Paolesse: Chemical Sensitivity of Porphyrin Assemblies. *Materials Today* **13(7-8)**, 46-52, (2010).

10 J.-S. Hu, H.-X. Ji, and L.-J. Wan: Metal Octaethylporphyrin Nanowire Array and Network toward Electric/Photoelectric Devices. *J. Phys. Chem. C* **113**, 16259-16265, (2009).

11 M. Jurow, A.E. Schuckman, J.D. Batteas, and C.M. Drain: Porphyrins as Molecular Electronic Components of Functional Devices. *Coord. Chem. Rev.* **254**, 2297-2310, (2010).

12 C. Li, J. Ly, B. Lei, W. Fan, D. Zhang, J. Han, M. Meyyappan, M. Thompson, and C. Zhou: Data Storage Studies on Nanowire Transistors with Self-Assembled Porphyrin Molecules. *J. Phys. Chem. B* **108**, 9646-9649, (2004).

13 E.M. Lupton, L. Chen, and F. Liu: Uniaxial Strain in Molecular Nanowires: A Case Study of β-phase Polyfluorenes. *J. Phys. Chem. Lett.* **1**, 1326–1331, (2010).

14 L. Adler-Abramovich, N. Kol, I. Yanai, D. Barlam, R.Z. Shneck, E. Gazit, and I. Rousso: Self-Assembled Organic Nanostructures with Metallic-Like Stiffness. *Angew. Chem. Int. Ed.* **49**, 9939 –9942, (2010).

15 F. Banhart: Interactions Between Metals and Carbon Nanotubes: at the Interface Between Old and New Materials. *Nanoscale* **1**, 201-213, (2009).

16 S. Guozhen and C. Di: One-Dimensional Nanostructures for Photodetectors. *Recent Patents on Nanotechnology* **4**, 20-31, (2010).

17 H. Xi, D.Z. Wei, W. Xu, and D. Zhu: Facile Method for Fabrication of Nanostructured CuPC Thin Films to Enhance Photocurrent Generation. *J. Phys. Chem. C* **112**, 19934–19938, (2008).

18 C.A. Berven, V. Dobrokhotov, D.N. McIlroy, S. Chava, R. Abdelrahaman, A. Heieren, J. Dick, and W. Barredo: Gas Sensing with Mats of Gold-Nanoparticle Decorated GaN Nanowires. *IEEE Sensors Journal* **2008**, *9*, 930-935.

19 D.K. Avasthi, A. Kumar, R. Singhal, A. Tripathi, and D.S.J. Misra: Studies on Carbon Nanotubes and Fullerenes Under Extreme Conditions. *J. Nanosci. Nanotech.* **10**, 3767-3779, (2010).

20 A.Z. Moshfegh: Nanoparticle Catalysts. *J. Phys. D* **42**, 233001/1-233001/30, (2009).

21 Z. Wang, C.J. Medforth, and J.A. Shelnutt: Porphyrin Nanotubes by Ionic Self-Assembly. *J. Am. Chem. Soc.* **126**, 15954-15955, (2004).

22 C.F.J. Faul and M. Antonietti: Ionic Self-Assembly: Facile Synthesis of Supramolecular Materials. *Adv. Mater.* **15**, 673–683, (2005).

23 Z. Wang, K.J. Ho, C.J. Medforth, and J.A. Shelnutt: Porphyrin Nanofiber Bundles from Phase-Transfer Ionic Self-Assembly and Their Photocatalytic Self-Metallization. *Adv. Mater.* **18**, 2557-2560, (2006).

24 J.-S. Hu, Y.-G. Guo, H.-P. Liang, L.-J. Wan, and L. Jiang: Three-dimensional Self-organization of Supramolecular Self-assembled Porphyrin Hollow Hexagonal Nanoprisms. *J. Am. Chem. Soc.* **127**, 17090-17095, (2005).

25 S.M. Yoon, I.-C. Hwang, K.S. Kim, and H.C. Choi: Synthesis of Single-Crystal Tetra(4-pyridyl)porphyrin Rectangular Nanotubes in the Vapor Phase. *Angew. Chem. Int. Ed.* **48**, 2506-2509, (2009).

26 C.J. Medforth, Z. Wang, K.E. Martin, Y. Song, J.L. Jacobsen, J.A. Shelnutt: Self-assembled Porphyrin Nanostructures. *Chem. Comm*. 7261-7277, (2009).

27 A.D. Schwab, D.E. Smith, C.S. Rich, E.R. Young, W.F. Smith, and J.C. de Paula: Porphyrin Nanorods. *J. Phys. Chem. B* **107**, 11339-11345, (2003).

28 J.R. Eskelsen, Y. Wang, Y. Qi, M. Ray, M. Handlin, K.W. Hipps, and U. Mazur: Protonation State of Core Nitrogens in the *Meso*-tetra(4-carboxyphenyl)porphyrin Impacts the Chemical and Physical Properties of Nanostructures Formed in Acid Solutions**.** *J. Porph. Phthal.* **16**, 1233–1243, (2012).

29 B.A. Friesen, B.C. Wiggins, J.L McHale, U. Mazur, and K.W. Hipps: A Self-Assembled Two-Dimensional Zwitterionic Structure: H6TSPP Studied on Graphite *J. Phys. Chem. C* **115**, 3990-3999, (2011).

30 C.M. Drain, A. Varotto, and I. Radivojevic: Self-Organized Porphyrinic Materials. *Chem. Rev*. **109**, 1630-1658, (2009).

31 B.A. Friesen, B. Wiggins, J. McHale, U. Mazur, and K.W. Hipps: Differing HOMO and LUMO Mediated Conduction in a Porphyrin Nanorod. *J. Amer. Chem. Soc*. **132**, 8554–8556, (2010).

32 Y. Tian, M.C. Beavers, T. Busani, K.E. Martin, J.L. Jacobsen, B.Q. Mercado, B.S. Swartzentruber, F. van Swol, C.J. Medforth, and J.A. Shelnutt: Binary Ionic Porphyrin Nanosheets: Electronic and Light-harvesting Properties Regulated by Crystal Structure. *Nanoscale* **4**, 1695–1700, (2012).

33 S. Liu, W. M. Wang, A. L. Briseno, S. C. B. Mannsfeld, and Z. Bao: Controlled Deposition of Crystalline Organic Semiconductors for Field-Effect-Transistor Applications. *Adv. Mater.* **21**, 1217-1232, (2009).

34 A. L. Briseno, S. C. B. Mannsfeld, X. Lu, Y. Xiong, S. A. Jenekhe, Z. Bao, and Y. Xia: Perylenediimide Nanowires and Their Use in Fabricating Field-Effect Transistors and Complementary Inverters. *Nano Lett. 7*, 668-675, (2007).

35 R. Li, W. Hu, Y. Liu, and D. Zhu: Nanoribbon Waveguides for Subwavelength Photonics Integration. *Science* **305**, 1269-1273, (2004).

36 K. E. Martin, Z. Wang, T. Busani, R.M. Garcia, Z. Chen, Y. Jiang, Y. Song, J.L. Jacobsen, T.T. Vu, N.E. Schore, B.S. Swartzentruber, C.J. Medforth, and J.A. Shelnutt: Donor-Acceptor Biomorphs from the Ionic Self-Assembly of Porphyrins. J. Am. Chem. Soc. ***132****, 8194-8201, (2010).*

37 W.M. Hikal and H.J. Harmon: Photocatalytic Self-assembled Solid Porphyrin Microcrystals from Water-soluble Porphyrins: Synthesis, Characterization and Application. Polyhedron ***28****, 113-120, (2009).*

38 V. Snitka, V. Mizariene, I. Bruzaite, V. Lendraitis, and M. Rackaitis: Synthesis and Characterization of Porphyrin Nanotubes Obtained by Ionic Self-assembly. *Int. J. Nanomanufacturing* **5**, 194-204, (2010).

39 K. Davami,. B. Mortazavi, H.M. Ghassemi, R.S. Yassar, J-S. Lee, Y. Remondc and M. Meyyappan: A computational and experimental investigation of the mechanical propertiesof single ZnTe nanowires. *Nanoscale* **4**, 897-903, (2012).

40 B. H. Toby: CMPR - a powder diffraction toolkit. *Journal of Applied Crystallography* **38**, 1040-1041, (2005).

41 A. Le Bail, H. Duroy, and J. L. Fourquet: Ab-initio Structure Determination of LiSbWO6 by X-Ray Powder Diffraction. *Mater. Res. Bull.* **23**, 447-452, (1988).

42 A. C. Larson and R. B. Von Dreele: General Structure Analysis System (GSAS), Los Alamos National Laboratory, Report LAUR 86±748, (2000).

43 B. H. Toby: *EXPGUI*, a Graphical User Interface for *GSAS*. *J. Appl. Cryst.* **34**, 210-213, (2001).

44 P. Thompson, D. E. Cox, and J. B. Hasting: Rietveld Refinement of Debye-Scherrer Synchrotron X-ray Data from Al2O3. *J. Appl. Crystallogr.* **20**, 79-83, (1987).

45 L. W. Finger, D. E. Cox, and A. P. Jephcoat: A Correction for Powder Diffraction Peak Asymmetry Due to Diaxial Divergence *J. Appl. Crystallogr.* **27**, 892-900, (1994).

46 CrystalMaker Software Ltd, Oxford, England (www.crystalmaker.com)

47 M.M Kruk and S.E. Braslavsky: Acid-Base Equilibria in 5,10,15,20-Tetrakis(4-sulfonatophenyl)chlorin: Role of Conformational Flexibility *J. Phys. Chem. A* **110**, 3414-3425, (2006).

48 E.B. Fleischer and L.E. Webb: The Basicity in Water of α,β,γ,δ-Tetra–(4-pyridyl)-porphine. *Inorg. Chem.* **67**, 1131-1133, (1963).

49 J.P. Macquet, M.M. Millard, and T. Theophanide: X-Ray Photoelectron Spectroscopy of Porphyrins. *J. Amer. Chem. Soc.* **100**, 4741-4746, (1978).

50 L. Yang, J. Xiao, T.E. Shubina, M. Chen, Z. Shi, M. Schmid, H.-P. Steinruck, J.M. Gottfried, and N. Lin: Coordination and Metalation Bifunctionality of Cu with 5,10,15,20-Tetra(4-pyridyl)porphyrin: Toward a Mixed-Valence Two-Dimensional Coordination Network. *J. Am. Chem. Soc.* **134**, 6401-6408, (2012)

51 Y. Zubavichus, M. Zharnikov, Y. Yang, O. Fuchs, E. Umbach, C. Heske, A. Ulman, and M. Grunze: X-ray Photoelectron Spectroscopy and Near-Edge X-ray Absorption Fine Structure Study of Water Adsorption on Pyridine-Terminated Thiolate Self-Assembled Monolayers. *Langmuir* **20**, 11022-11029, (2004).

52 A. Borras, O. Groning, M. Aguirre, F. Gramm, and P. Groning: One-Step Dry Method for the Synthesis of Supported Single-Crystalline Organic Nanowires Formed by π-Conjugated Molecules. *Langmuir* **26**, 5763–5771, (2010).

53 P.S. Pershan: Scattering from Mesomorphic Structures. *International Tables for Crystallography* **B**, 547–566, (2010).

54 D.B. Williams and C.B. Carter. *Transmission Electron Microscopy: A Textbook for Materials Science.* (Springer Science + Business Media, LLC., New York, 1996) pp.165-167.

55 Z.M. Ou, H. Yao, and K. Kimura: Preparation and Optical Properties of Organic Nanoparticles of Porphyrin Without Self-aggregation. *J. Photochem. Photobiol. A:Chem.* **189**, 7-14, (2007).

56 W.M. Hikal and H.J. Harmon: Photocatalytic Self-assembled Solid Porphyrin Microcrystals from Water-soluble Porphyrins: Synthesis, Characterization and Application. *Polyhedron* **28**, 113-120, (2009).

57 A. Amunts, O. Drory, and N. Nelson: The Structure of a Plant Photosystem I Supercomplex at 3.4 Å Resolution. Nature ***447, 58-63, (2007).***

58 B. V. Derjaguin, V. M. Muller, and YU. P. Toporov: Effect of Contact Deformations on the Adhesion of Particles. *Journal of Colloid and Interface Science* **53(2)**, 314-326, (1975).

59 I. N. Sneddon: The Relation between Load and Penetration in the Axisymmetric Boussinesq Problem for a Punch of Arbitrary Profile. *Int. J. Engng. Sci.* **3**, 47-57 (1965).

60 K. L. Johnson, K. Kendall and A. D. Roberts: Surface Energy and the Contact of Elastic Solids. *Proc. R. Soc. Lond. A.* **324**, 301-313 (1971).

61 M. Radmacher: Measuring the Elastic Properties of Biological Samples with the AFM. *IEEE Eng. Med. Biol. Mag.* **16**, 47-57 (1997).

62 W. C. Oliver and G. M. Pharr: An Improved Technique for Determining Hardness and Elastic Modulus Using Load and Displacement Sensing Indentation Experiments. *Journal of Materials Research* **7(6)**, 1546-1583, (1992).

63 T. Oshiro, A. Backstrom, A.-M. Cumberlidge, K. W. Hipps, U. Mazur, S. P. Pevovar, D. F. Bahr, and J. Smieja: Nanomechanical Properties of ordered Phthalocyanine Langmuir-Blodgett Layers. *Journal of Materials Research* **19(5)**, 1461-1470, (2004).

64 J. E. Sader, J. W. M. Chon, and P. Mulvaney: Calibration of Rectangular Atomic Force Microscope Cantilevers. *Review of Scientific Instruments* **70(10)**, 3967-3969, (1999).

65 M. E. Dokukin and I. Sokolov: On the Measurements of Rigidity Modulus of Soft Materials in Nanoindentation Experiments at Small Depth. *Macromolecules* **45**, 4277-4288, (2012).

66 M. Dokukin and I. Sokolov: Quantitative Mapping of the Elastic Modulus of Soft Materials with HarmoniX and PeakForce QNM AFM Modes. *Langmuir* **28**, 16060-16071, (2012).

67 PF-QNM User Guide Rev F., Bruker Corporation, 51, (2009).

68 T. Tsuji and K. Yamanaka: Observation by Ultrasonic Atomic Force Microscopy of Reversible Displacement of Subsurface Dislocations in Highly Ordered Pyrolytic Graphite. *Nanotechnology* **12**, 301-307, (2001).

69 D. M. Schaefer, A. Patil, R. P. Andres, and R. Reifenberger: Measuring the Mechanical Properties of Preformed, Nanometer-size Gold Clusters with the Atomic Force Microscope. In Atomic Force Microscopy/scanning Tunneling Microscopy; S. H. Cohen, Mona T. Bray, and M. L. Lightbody, Ed.; Plenum Press: New York, 411-421, (1994).

70 K. Yamanaka, T. Tsuji, A. Noguchi, T. Koike, and T. Mihara: Nanoscale Elasticity Measurement with in situ Tip Shape Estimation in Atomic Force Microscopy. *Review of Scientific Instruments* **71**, 2403-2408, (2000).

[71] M. Gandhi, G.M. Spinks, R.P. Burford, and G.G. Wallace: Film Structure and Mechanical Properties of Electrochemically Prepared Polypyrrole. *Polymer* **36**, 4761-4765, (1995).

[72] V. Jardret, H. Zahouani, J. L. Loubet, and T. G. Mathia: Understanding the Quantification of Elastic and Plastic Deformation During a Scratch Test. *Wear* **218**, 8-14, (1998).

[73] M. Kanari, H. Kawamata, T. Wakamatsu, I. Ihara: Intermolecular Elastic and Plastic Characteristics of Organic Phthalocyanine Thin Films Evaluated by Nanoindentation. *Appl. Phys. Lett.* **90**, 061921, (2007).

[74] G. Simmons and H. Wang: Single Crystal Elastic Constants and Calculated Aggregate Properties: A Handbook, 2nd ed. *The MIT Press,* Cambridge, Massachusetts and London England, 304-309 (1971).

[75] A. Floresa, F. J. Balta Calleja, G. E. Attenburrow, and D. C. Bassett: Microhardness Studies of Chain-extended PE: III. Correlation with Yield Stress and Elastic Modulus. *Polymer* **41**, 5431-5435, (2000).

 This journal is © The Royal Society of Chemistry [year]